Science Press   Springer-Verlag

Utilizing sediment grain size characteristics to assess the effectiveness of clay–sand barriers in reducing aeolian erosion in Minqin desert area, China

SONG Dacheng[1,2], ZHAO Wenzhi[1,3*], LI Guangyu[2], WEI Lemin[3], WANG Lide[1,2], YANG Jingyi[1], WU Hao[2], MA Quanlin[1]

[1] College of Forestry, Gansu Agricultural University, Lanzhou 730070, China;
[2] Gansu Hexi Corridor Forest Ecosystem National Research Station, Gansu Desert Control Research Institute, Lanzhou 730070, China;
[3] Linze Inland River Basin Research Station, Northwest Institute of Eco-Environment and Resources, Chinese Academy of Sciences, Lanzhou 730000, China

Abstract: The clay–sand barriers in Minqin desert area, China, represent a pioneering windbreak and sand fixation project with a venerable history of 60 a. However, studies on evaluating the long-term effectiveness of clay–sand barriers against aeolian erosion, particularly from the perspective of surface sediment grain size, are limited and thus insufficient to ascertain the protective impact of these barriers on regional aeolian activities. This study focused on the surface sediments (topsoil of 0–3 cm depth) of clay–sand barriers in Minqin desert area to explain their erosion resistance from the perspective of surface sediment grain size. In March 2023, six clay–sand barrier sampling plots with clay–sand barriers of different deployment durations (1, 5, 10, 20, 40, and 60 a) were selected as experimental plots, and one control sampling plot was set in an adjacent mobile sandy area without sand barriers. Surface sediment samples were collected from the topsoil of each sampling plot in the study area in April 2023 and sediment grain size characteristics were analyzed. Results indicated a predominance of fine and medium sands in the surface sediments of the study area. The deployment of clay–sand barriers cultivated a fine quality in grain size composition of the regional surface sediments, increasing the average contents of very fine sand, silt, and clay by 30.82%, 417.38%, and 381.52%, respectively. This trend became markedly pronounced a decade after the deployment of clay–sand barriers. The effectiveness of clay–sand barriers in erosion resistance was manifested through reduced wind velocity, the interception of sand flow, and the promotion of fine surface sediment particles. Coarser particles such as medium, coarse, and very coarse sands predominantly accumulated on the external side of the barriers, while finer particles such as fine and very fine sands concentrated in the upwind (northwest) region of the barriers. By contrast, the contents of finest particles such as silt and clay were higher in the downwind (southeast) region of the sampling plots. For the study area, the deployment of clay–sand barriers remains one of the most cost-effective engineering solutions for aeolian erosion control, with sediment grain size parameters serving as quantitative indicators for the assessment of these barriers in combating desertification. The results of this study provide a theoretical foundation for the construction of windbreak and sand fixation systems and the optimization of artificial sand control projects in arid desert areas.

Keywords: clay–sand barriers; sediment grain size; grain size distribution; aeolian erosion; windbreak and sand fixation; Minqin desert area

1 Introduction

Desertification has emerged as a major ecological issue in China (Pan et al., 2020). Data from the sixth national monitoring survey on desertification revealed that the sandified land area in China covered 1.6878×10^6 km^2 as of 2019, accounting for 65.58% of the total desertified land area and 17.58% of the total area in China (Meng et al., 2023). Despite controlled expansion of desertification, the ecological environment in arid and semi-arid areas remains sensitive and fragile, and the situation regarding desertification and sand control remains severe (Cui et al., 2023). Over the years, engineering and biological measures have been proven to be the most cost-effective and sustainable methods in the desertification control technology system of China, with several successful model implementations in different arid and semi-arid areas (Li et al., 2004; Cao et al., 2007). However, large-scale afforestation for sand control is not feasible in regions prone to severe wind and sand disasters or water resource shortages. The deployment of sand barriers in these areas has become the primary method for sand control (Wang et al., 2017). Sand barriers are characterized by their capability to weaken wind speed, stabilize the sand surface, increase the aerodynamic roughness of the ground surface, and effectively control the movement of sand particles within the barriers. These barriers can also obstruct wind–sand flow, reduce the sand-carrying capacity of the wind, and promote the settling of wind–sand flow, thereby controlling their movement. Additionally, the settling of fine particles within the barriers facilitates soil particle refinement, which is conducive to vegetation restoration (Burno et al., 2018; Ding et al., 2018a).

In arid areas, soil aeolian erosion has emerged as one of the primary factors accelerating land degradation and desertification (Labiadh et al., 2023). The interaction between wind and surface particles mainly affects the soil aeolian erosion process. Aeolian erosion occurrence is closely related to the grain size composition of the surface soil, which not only determines its motion state but also affects the intensity of aeolian erosion (Dong and Li, 1998). Sediment transportation and deposition processes, as well as the interaction between aeolian erosion and underlying surface particles, are characterized by spatial differences in grain size composition and distribution. Therefore, grain size analysis has become an important tool for desert research due to its simplicity, accessibility, and sensitivity to environmental changes (Song et al., 2016). Researchers increasingly depend on grain size parameters such as mean grain size, skewness, kurtosis, frequency distribution curve, cumulative frequency distribution curve, and source function, to assess regional wind and sand activities, infer sediment environments, and provide information regarding sediment sources (Qiao et al., 2006; Zhang and Dong, 2012; Dong et al., 2022).

Sand barriers, developed over several years, have become a relatively effective measure against aeolian erosion in arid areas (Bruno et al., 2018). Sand barriers typically adhere to the principle of utilizing local materials without extensive processing. This approach not only reduces costs but also promotes efficient resource utilization, making it a promising future development trend (Wang et al., 2020). Clay–sand barriers are the primary sand control means employed in large-scale sand control projects in the inland sand areas of Northwest China due to their affordability and availability, environmental friendliness, water retention capacity, aeolian erosion resistance, and easy construction (Wang et al., 2020). Clay–sand barriers, which are impermeable to wind, are often made from locally sourced clay with adhesive properties, manually stacked into earth embankments, and laid on the surface of mobile sand areas. Moreover, clay–sand barriers are mostly constructed in a belt-like manner, perpendicular to the main regional wind direction. Investigating the sand fixation effect of clay–sand barriers is crucial for optimizing regional sand barrier types and holds remarkable value for desertification control and ecological environmental construction in arid desert areas.

Minqin desert area is a representative region for sand control efforts in China, where substantial contributions have been made to the sand control work that can reflect the progress and level of sand control of China to some extent. However, research on clay–sand barriers since their inception in the 1960s has been sparse, primarily focusing on construction methods, cost accounting, and the effects of vegetation restoration (Chang et al., 2000). Previous studies have confirmed that clay–sand barriers are initially effective in windbreak and sand fixation, with the sediment transport rate at 0–20 cm depth near the surface of the barriers being 19.32% of that in mobile sand areas; however, this rate increased to 30.87% of that in mobile sand areas after 6 a of the deployment of clay–sand barriers (Sun et al., 2012). Plant community diversity within the barriers substantially surpassed that in mobile sand areas after 12 a of the deployment of clay–sand barriers (Ding et al., 2018). The damage rate caused by aeolian erosion processes to straw and plastic net barriers in mobile sand areas reached 8.50% and 17.65%, respectively, whereas the impact on clay–sand barriers was negligible, at less than 2.00% (Ma et al., 2013). In contrast to the less satisfactory performance of straw and nylon grid barriers, clay–sand barriers have been widely adopted in the cold sandy regions of the Gonghe Basin in China due to their lowest comprehensive cost and superior sand control effectiveness (Wang et al., 2020). However, research on the resistance of clay–sand barriers to aeolian erosion is exceedingly limited, rarely conducting assessments on their performance from the perspective of surface sediment grain size or performing comparative evaluations over different deployment durations. Such research is insufficient to clarify the protective effect of clay–sand barriers against regional aeolian activity.

Therefore, this study aims to address this research gap by investigating the clay–sand barrier sand fixation area in Minqin desert area, which has experienced nearly 60 a of the deployment of clay–sand barriers. This study posited the following scientific hypotheses: (1) clay–sand barriers with varying deployment durations can influence the grain size distribution of surface sediments; and (2) clay–sand barriers can affect the spatial distribution of sediments by altering aeolian erosion processes. The current study analyzed the characteristics of sediment grain size, grain size parameters, and grain size frequency distribution curves of surface sediments in the clay–sand barriers with different deployment durations through field investigations and control experiments to address the aforementioned objectives. From the perspective of sediment grain size within the clay–sand barriers, this study elucidated the sand-fixing effects and temporal efficacy of the barriers. The results will help establish a theoretical basis for enhancing and sustainably developing artificial sand control projects in comparable arid desert areas.

2 Materials and methods

2.1 Study area

The study area (38°34′–38°37′N, 102°55′–102°58′E) is situated in Minqin desert area on the southeastern edge of the Badain Jaran Desert, Northwest China. Prior to the Han Dynasty, vast water bodies existed in the region; however, since the Han Dynasty, the ecological environment has gradually deteriorated, leading to increasing desertification. The environment exhibits a typical temperate continental arid desert climate, with an average annual temperature of 7.6°C, a frost-free period of 176 d, an average annual precipitation of 110 mm (mainly concentrated from July to September, accounting for approximately 60% of the total annual precipitation), and an average annual evaporation of approximately 2600 mm, which is 23 times higher than the annual precipitation. The groundwater level is approximately 16–20 m deep. The region experiences strong wind and sand activities, with the northwest wind acting as the dominant wind direction (Fig. 1). The average annual wind speed is 2.5 m/s, with an average of 25.1 d with wind, 25.6 d with sandstorm, and 27.8 d with wind speeds over eight levels (Zhao et al., 2023). The main soil types include gray-brown desert soil, non-zonal aeolian soil, and meadow soils. The desert vegetation in the area exhibits distinct characteristics, with a simple community structure primarily comprising drought-resistant shrubs, semi-shrubs, and herbs. Dominant plant species include

Haloxylon ammodendron, *Reaumuria songarica*, *Nitraria tangutorum*, *Calligonum mongolicum*, *Artemisia arenaria*, *Agriophyllum squarrosum*, and *Salsola collina* (Man et al., 2023).
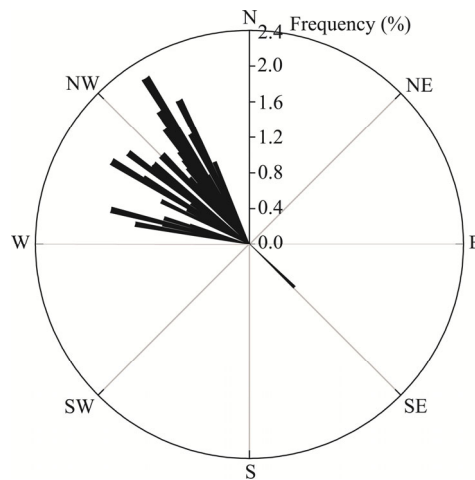

Fig. 1 Wind direction rose of the study area from 2018 to 2022. N, north; NE, northeast; E, east; SE, southeast; S, south; SW, southwest; W, west; NW, northwest. Data were from the Gansu Minqin National Studies Station for Desert Steppe Ecosystem, and all data were monitored at wind speeds greater than 0.5 m/s.

2.2 Experimental design and soil sampling

In March 2023, six clay–sand barrier sampling plots with different deployment durations (1, 5, 10, 20, 40, and 60 a) were selected as experimental plots in the northwest of the Minqin Sand Control Comprehensive Experimental Station. The control sampling plot was in an adjacent mobile sandy area without sand barriers (Table 1; Fig. 2a). Each sampling plot was flat, with similar elevations and landforms. The clay–sand barriers in the study area comprise locally sourced clay with adhesive properties from Minqin County and are organized in a belt-like manner perpendicular to the dominant regional wind direction, with a barrier height of approximately 30 cm and a row spacing of 3 m (Fig. 2b and c). Each clay–sand barrier has been in use since its initial deployment and has not undergone any repairs during this period. In April 2023, surface sediment samples were collected from the topsoil (0–3 cm depth) of each sampling plot in the study area (Fig. 2c). Three sampling points (corresponding to three positions) were selected within each clay-sand barrier sampling plot: northwest (upwind), middle, and southeast (downwind) (Fig. 2d). Five replicated samples were then randomly collected from each sampling point and mixed on-site and stored in plastic self-sealing bags. Only five replicated soil samples were collected from the control sampling plot.

2.3 Measurement of sediment grain size

Sediment sample preparation and grain size measurements were performed at the State Key Laboratory Breeding Base for Desertification and Aeolian Sand Disaster Combating in Wuwei City, China. All samples were air dried, sieved to remove impurities, and then subjected to organic matter removal and desalination treatment. Sediment grain size measurements were performed using the wet method with the Mastersizer 2000 laser grain size analyzer (Malvern, Worcestershire, UK). The measurement range of the instrument was 0.020–2000.000 μm, and the measurements were repeated three times with an error of less than 2%. The specific pretreatment method was as follows: a certain amount of sample was weighed in accordance with the soil type and then 10 mL of 10% H_2O_2 was added. The mixture was heated and boiled until no bubbles were produced to remove organic matter and easily oxidizable salt substances. After cooling, 10 mL of 10% hydrochloric acid was added and shaken at a low temperature to remove calcium salts. The mixture was then left to stand for more than 12 h in distilled water. Next, 10 mL of 10% sodium hexametaphosphate was added to the sample, and the mixture was dispersed for 30 s using ultrasonic waves before proceeding with the subsequent measurements.

Table 1   Detailed information of the sampling plots

Deployment duration (a)	Latitude (N)	Longitude (E)	Altitude (m)	Sand barrier specification
0	38°36′39″	102°57′24″	1324	Mobile sand without sand barrier
1	38°35′59″	102°57′28″	1321	Belt clay–sand barrier
5	38°37′34″	102°55′40″	1318	Belt clay–sand barrier
10	38°36′35″	102°57′22″	1320	Belt clay–sand barrier
20	38°36′10″	102°57′45″	1322	Belt clay–sand barrier
40	38°36′01″	102°57′53″	1317	Belt clay–sand barrier
60	38°34′49″	102°58′30″	1330	Belt clay–sand barrier
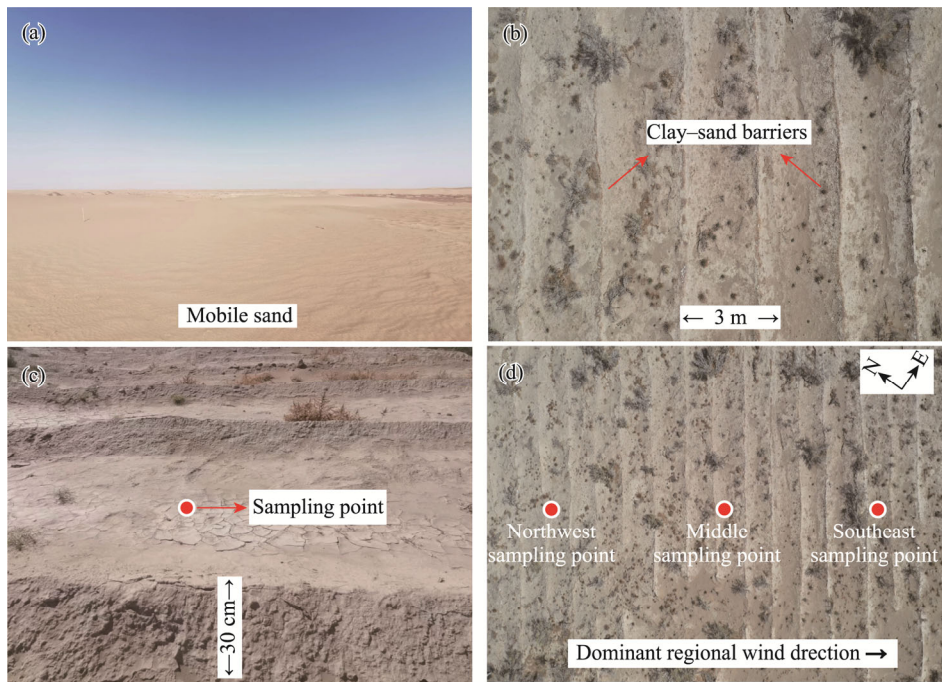
Fig. 2   Photographs showing the control sampling plot (a), clay–sand barrier sampling plots (b and c), and three sampling points within an clay–sand barrier sampling plot (d)

In terms of sediment grain size classification, this study adopted the US standard for surface sediment grain size classification (Zhao et al., 2023). The sediment particle components were classified as follows: gravel (>2.000 mm), very coarse sand (1.000–2.000 mm), coarse sand (0.500–1.000 mm), medium sand (0.250–0.500 mm), fine sand (0.100–0.250 mm), very fine sand (0.050–0.100 mm), silt (0.002–0.050 mm), and clay (<0.002 mm). Grain size data were analyzed in Excel 2010, SPSS 23.0, and Origin 2021.

2.4   Calculation of the grain size parameters

Grain size parameters were calculated using the formulas developed by Folk and Ward (1957), and the grading standard of grain size parameters is shown in Table 2. Grain size was measured in phi (Φ) unit ($\Phi = -\log_2 d$, where d is the grain size in mm) and described using mean grain size (M_z; Φ), sorting (σ), skewness (S_K), and kurtosis (K_G), which were determined using the following formulas:

$$M_z = \frac{1}{3}(\Phi_{16} + \Phi_{50} + \Phi_{84}),$$ (1)

$$\sigma = \frac{1}{4}(\Phi_{84} - \Phi_{16}) + \frac{1}{6.6}(\Phi_{95} - \Phi_5),$$ (2)

$$S_K = \frac{\Phi_{16} + \Phi_{84} - 2\Phi_{50}}{2(\Phi_{84} - \Phi_{16})} + \frac{\Phi_5 + \Phi_{95} - 2\Phi_{50}}{2(\Phi_{95} - \Phi_5)}, \tag{3}$$

$$K_G = \frac{\Phi_{95} - \Phi_5}{2.44(\Phi_{75} - \Phi_{25})}, \tag{4}$$

where Φ_{16}, Φ_{50}, Φ_{84}, Φ_{95}, Φ_5, Φ_{72}, and Φ_{25} are grain size values (Φ) for representative cumulative percentages of 16%, 50%, 84%, 95%, 5%, 72%, and 25%, respectively.

Table 2 Grading standards of selected grain size parameters

M_z (Φ)		σ		S_K		K_G	
Range	Definition	Range	Definition	Range	Definition	Range	Definition
>8	Clay	<0.35	Extremely good	−1.00– −0.30	Very negative skewed	<0.67	Very platykurtic
4–8	Silt	0.35–0.50	Good	−0.30– −0.10	Negative skewed	0.67–0.90	Platykurtic
3–4	Very fine sand	0.50–0.71	Better	−0.10–0.10	Near symmetrical	0.90–1.11	Mesokurtic
2–3	Fine sand	0.71–1.00	Medium	0.10–0.30	Positive skewed	1.11–1.56	Leptokurtic
1–2	Medium sand	1.00–2.00	Worse	0.30–1.00	Very positive skewed	1.56–3.00	Very leptokurtic
0–1	Coarse sand	2.00–4.00	Bad			>3.00	Extremely leptokurtic
<0	Very coarse sand	>4.00	Worst				

Note: M_z, mean grain size; σ, sorting; S_K, skewness; K_G, kurtosis.

3 Results

3.1 Sediment grain size distribution

All the surface sediment samples in the study area primarily comprised fine sand (38.85% of the volume) and medium sand (25.65%), followed by very fine sand (12.85%) and coarse sand (8.81%), with little contents of other components. The clay–sand barriers had a significant impact on the contents of fine sand, silt, and clay components in the regional surface sediments; compared to the mobile sand area, the average contents of silt and clay in the surface sediments of clay–sand barrier sampling plots were 4.17 and 3.78 times higher, respectively, while the average content of fine sand decreased by 26.51% (Table 3).

Considerable differences existed in the grain size distribution of surface sediments across various clay–sand barrier sampling plots. With the increasing duration since deployment, a general declining trend in fine sand content and a fluctuating rise in silt and clay contents were observed. Key temporal milestones were observed at 1, 10, and 60 a after the deployment of clay–sand barriers. At the 1 a mark, the average contents of silt and clay in the surface sediments of clay–sand barrier sampling plots were 14.70% and 2.94%, respectively, representing increases of 502.46% and 476.47%, respectively, over the mobile sand area. After 10 a of the deployment of clay–sand barriers, the average contents of silt and clay slightly decreased by approximately 30.00%, while the content of very fine sand significantly increased, more than doubling, possibly due to partial damage of clay–sand barriers over time, which compromised their protective function. Among all clay–sand barrier sampling plots, the plot where the clay–sand barriers deployed for 60 a exhibited the largest contrast with mobile sand area, which were characterized by a substantial increase in fine particle content and a significant decrease in coarse particle content. Despite serious damage to some sections of clay–sand barriers, the development of a mature plant community system and the formation of surface soil crusts after 60 a ensured a continuous, stable effect from barriers in windbreak and sand fixation.

Regardless of differences in the grain size distribution of surface sediments among different positions within the clay–sand barrier sampling plots, the overall grain size distribution followed

the grain size distribution in the dominant regional wind direction (Table 3). The differences in the grain size distribution of surface sediments between the upwind and downwind regions within the clay–sand barrier sampling plots were highly pronounced. Except for the slightly higher content of fine sand (mean of 53.78%) in the surface sediments of clay–sand barrier sampling plot (deployment duration of 1 a) in the upwind region compared to that in the mobile sand area (mean of 50.28%), the contents of fine sand in the surface sediments of the other clay–sand barrier sampling plots were significantly lower than that in the mobile sand area, demonstrating a reduction ranging from 8.97% to 58.05%. Similar to fine sand, the average content of very fine sand in the surface sediments of all the clay–sand barrier sampling plots was higher in the upwind region (15.09%) and lower in the downwind region (12.54%). In contrast to fine and very fine sands, the average contents of silt and clay in the surface sediments of all the clay–sand barrier sampling plots displayed a decreasing trend from the downwind region (3.47% and 16.11%, respectively) to the middle region (2.33% and 12.92%, respectively) and then to the upwind region (1.51% and 8.84%, respectively). The differences in the contents of medium and coarse sands among different positions were insignificant. Furthermore, among all the clay–sand barrier sampling plots, the clay–sand barrier sampling plot with deployment duration of 60 a exhibited the smallest variation in grain size distribution among different positions, indicating a highly stable surface sediment environment.

Table 3 Surface sediment grain size distribution at different positions of each clay–sand barrier sampling plot

Sampling plot		Sediment grain size distribution (%)						
Deployment duration (a)	Position	Clay (<0.002 mm)	Silt (0.002–0.050 mm)	Very fine sand (0.050–0.100 mm)	Fine sand (0.100–0.250 mm)	Medium sand (0.250–0.500 mm)	Coarse sand (0.500–1.000 mm)	Very coarse sand (>1.000 mm)
0	/	0.51±0.05	2.44±0.07	10.17±0.21	50.28±0.07	29.33±0.22	7.28±0.10	0.00±0.00
1	Upwind	0.18±0.00^{Eb}	2.51±0.02^{Ec}	7.57±0.10^{Eb}	53.78±0.51^{Aa}	31.27±0.44^{ABa}	4.69±0.22^{Da}	0.00±0.00^{Aa}
	Middle	4.29±0.02^{Ba}	19.92±0.54^{Bb}	8.77±0.54^{Da}	44.10±1.55^{Ab}	21.05±0.66^{Ec}	1.81±1.87^{Da}	0.06±0.11^{Ba}
	Downwind	4.35±0.41^{Ba}	21.66±1.07^{Ca}	6.91±0.35^{Db}	38.36±2.48^{Ac}	24.74±0.55^{Cb}	3.91±1.79^{CDa}	0.07±0.12^{Ba}
5	Upwind	1.28±0.04^{Ca}	4.57±0.13^{Da}	20.23±0.49^{Ba}	45.77±0.97^{Ba}	18.61±0.69^{Dc}	9.00±0.79^{Cc}	0.54±0.18^{Ab}
	Middle	1.04±0.02^{Cb}	4.36±0.06^{Ea}	14.01±0.32^{Bb}	35.72±0.76^{Cb}	24.05±0.12^{Db}	17.87±0.60^{Bb}	2.95±0.65^{Aa}
	Downwind	0.89±0.11^{Dc}	3.55±0.26^{Eb}	10.25±0.66^{Cc}	26.31±1.54^{Ec}	27.94±0.24^{Ba}	27.54±1.66^{Aa}	3.52±0.68^{Aa}
10	Upwind	2.03±0.05^{Bb}	8.84±0.04^{Bb}	17.93±0.26^{Ca}	45.36±0.38^{Ba}	22.68±0.32^{Cb}	3.16±0.47^{Db}	0.00±0.00^{Aa}
	Middle	0.98±0.03^{CDc}	6.11±0.11^{Cc}	10.63±0.32^{Cb}	39.63±0.67^{Bb}	35.72±0.56^{Ca}	6.92±0.57^{Ca}	0.00±0.00^{Ba}
	Downwind	3.33±0.02^{Ca}	15.16±0.34^{Da}	18.62±0.89^{Ba}	35.43±1.84^{Bc}	20.83±0.40^{Dc}	6.35±2.19^{Ca}	0.28±0.49^{Ba}
20	Upwind	0.96±0.06^{Da}	5.89±0.32^{Ca}	10.35±0.67^{Da}	34.91±1.84^{Dc}	31.61±0.34^{Ac}	15.87±2.29^{Aa}	0.40±0.44^{Aa}
	Middle	0.97±0.03^{CDa}	5.00±0.16^{DEb}	7.05±0.27^{Eb}	42.76±0.38^{Aa}	37.37±0.54^{Bb}	6.85±0.30^{Cc}	0.00±0.00^{Ba}
	Downwind	0.70±0.02^{DEb}	3.53±0.08^{Ec}	6.72±0.12^{Db}	38.56±0.79^{Ab}	39.10±0.40^{Aa}	11.39±0.65^{Bb}	0.00±0.00^{Ba}
40	Upwind	0.17±0.01^{Ec}	3.68±0.11^{Dc}	10.35±0.26^{Da}	43.29±0.88^{Ca}	30.39±0.05^{Bb}	11.97±1.05^{Bb}	0.16±0.17^{Aa}
	Middle	0.88±0.08^{Db}	5.48±0.25^{CDb}	4.82±0.11^{Fc}	27.14±0.65^{Dc}	39.88±0.36^{Aa}	21.58±1.02^{Aa}	0.22±0.13^{Ba}
	Downwind	7.03±0.19^{Aa}	25.45±0.68^{Ba}	9.67±0.17^{Cb}	31.78±0.25^{Cb}	21.09±0.88^{Dc}	4.97±0.48^{CDc}	0.00±0.00^{Ba}
60	Upwind	4.45±0.26^{Ab}	27.56±1.52^{Ab}	24.14±1.33^{Ab}	27.22±0.67^{Eb}	11.52±0.89^{Ea}	4.28±1.93^{Da}	0.82±1.43^{Aa}
	Middle	5.81±0.18^{Aa}	36.63±1.08^{Aa}	28.29±1.02^{Aa}	21.09±0.72^{Ec}	4.73±0.62^{Fc}	2.68±1.69^{Da}	0.77±1.33^{Ba}
	Downwind	4.54±0.13^{Bb}	27.33±0.95^{Ab}	23.07±0.78^{Ab}	33.86±0.95^{BCa}	8.01±0.50^{Eb}	2.35±1.30^{Da}	0.85±1.48^{Ba}

Note: '/' means no position. Values are mean±SD. Three positions were selected within each clay–sand barrier sampling plot: northwest (upwind), middle, and southeast (downwind). Capitalized superscript letters indicate significant differences at the same position in different clay–sand barrier sampling plots ($P<0.05$). Lowercase superscript letters indicate significant differences at different positions for the same clay–sand barrier sampling plot ($P<0.05$).

3.2 Sediment grain size parameters

Figures 3 and 4 show the mean grain size, sorting, skewness, and kurtosis of the surface

sediments in the study area. The surface sediments of clay–sand barrier sampling plots generally exhibited a finer mean grain size compared to the mobile sand area. The surface sediments of the mobile sand area demonstrated a mean grain size of 2.109 Φ, indicating fine sand. Conversely, the surface sediments of clay–sand barrier sampling plots exhibited a mean grain size range from 2.135 to 4.181 Φ, considerably greater than that of the mobile sand area. Throughout a 60-a deployment duration, compared to the mobile sand area, the mean grain size at all clay–sand barrier sampling plots showed an increasing trend (ranging from 1.25% to 98.25%), and the mean values presented a fluctuating upward trend as the duration extended. Surface sediments taken from the sampling plot with a 60-a deployment duration of clay–sand barriers displayed the smallest mean grain size (4.181 Φ) and the highest content of silt (30.51%). The analysis of surface sediments from different positions within the clay–sand barrier sampling plots showed that the mean grain size in the upwind, middle, and downwind regions was 2.645, 2.791, and 3.125 Φ, respectively, demonstrating a distinct refinement effect.

The sorting of surface sediments in the mobile sand area was 0.907, indicating medium sorting level. After the deployment of clay–sand barriers, the sorting exhibited a fluctuating upward trend as the duration extended, demonstrating average values ranging from 1.118 to 2.219, which were all higher than that in the mobile sand area. The higher values indicate that particle sorting of surface sediments in the clay–sand barrier sampling plots is poorer compared to that in the mobile sand area. Furthermore, particle sorting of surface sediments in the clay–sand barrier sampling plots gradually transitioned from worse (1–40 a after the deployment of clay–sand barriers) to bad (60 a after the deployment of clay–sand barriers) with the passage of time. Additionally, this study reveals a correlation between particle sorting of clay–sand barrier sampling plots in the study area and the dominant wind direction in the region. Compared to the middle and downwind regions, the upwind region showed superior particle sorting. The average values of sorting at the three positions were 1.338 in the upwind region, 1.564 in the middle region, and 1.947 in the downwind region.

The average value of skewness of surface sediments in the mobile sand area was –0.001, which is classified as "near symmetrical". After the deployment of clay–sand barriers, the surface sediments generally showed positive and very positively skewed, and the average values of skewness also significantly increased compared to the mobile sand area. The average values of skewness of surface sediments in the clay–sand barrier sampling plots with deployment durations of 1, 5, 10, 20, 40, and 60 a were 0.413 (very positively skewed), 0.047 (near symmetrical), 0.291 (positively skewed), 0.212 (positively skewed), 0.305 (very positively skewed), and 0.356 (very positively skewed), respectively. The variation trend of skewness between different positions was consistent with that of the main grain size, demonstrating the highest skewness in the downwind region (0.125), followed by the middle region (0.304), and the upwind region (0.383).

The kurtosis value of surface sediments in the mobile sand area was 0.985, which is classified as "mesokurtic" kurtosis. Except for the surface sediments in the clay–sand barrier sampling plot (deployment duration of 5 a) with a relatively low average value of kurtosis (0.954), the average values of kurtosis of surface sediments in the other clay–sand barrier sampling plots were higher than that of surface sediments in the mobile sand area, ranging from 1.086 to 1.473. This finding corresponded to "mesokurtic" and "leptokurtic" kurtosis levels. The results indicate that the clay–sand barriers can affect the grain size composition of surface sediments.

3.3　Frequency distribution curves

The grain size frequency distribution curves of surface sediments in the study area generally displayed a unimodal pattern, indicating effective particle sorting. In contrast to the surface sediments in the mobile sand area, the grain size frequency distribution curves of surface sediments in the clay–sand barrier sampling plots demonstrated a broader range of grain size distribution with flatter curves and deviations from the characteristics of a normal distribution. The majority of surface sediments in the clay–sand barrier sampling plots exhibited right-skewed grain size frequency distribution curves as opposed to the mobile sand area (Fig. 5). This finding
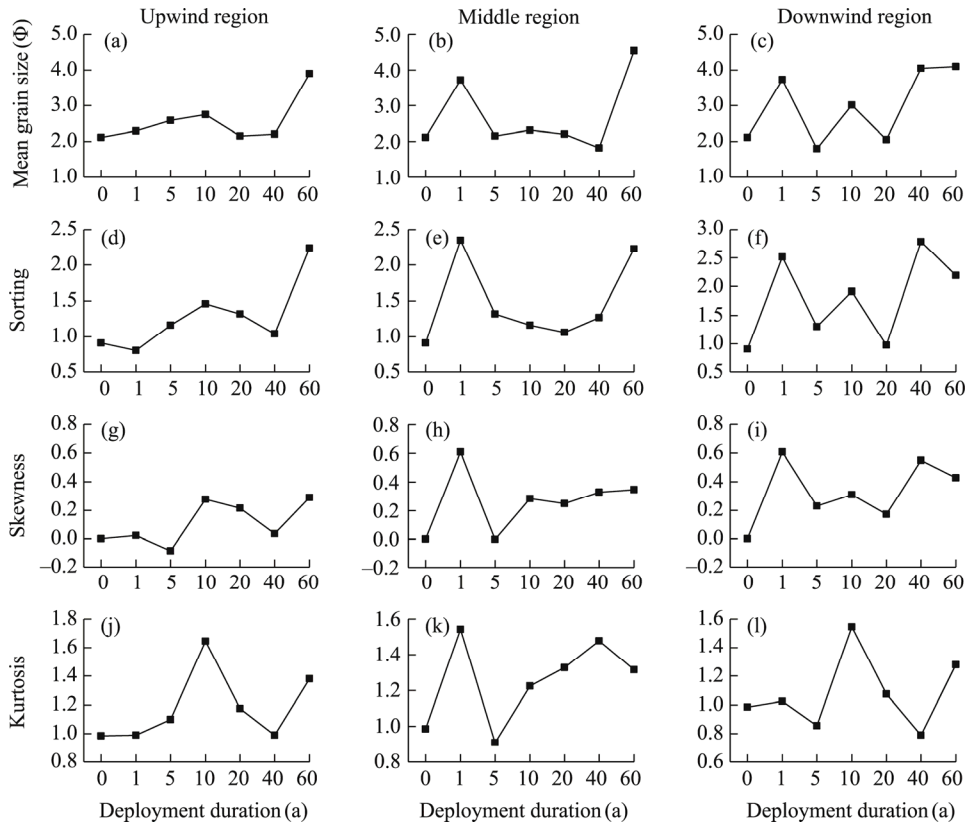
Fig. 3 Variations in mean grain size (a–c), sorting (d–f), skewness (g–i), and kurtosis (j–l) of surface sediments in the upwind (northwest), middle, and downwind (southeast) regions of different clay–sand barrier sampling plots. Note that the values for the control sampling plot in the mobile sandy area without clay–sand barrier (deployment duration of 0 a) have no differences in positions.

confirms the refining effect of the clay–sand barriers on the surface soil. After the deployment of clay–sand barriers, the primary grain size distribution range of surface sediments shifted from 0.060–4.250 Φ in the mobile sand area to 0.060–4.850 Φ in the clay–sand barrier sampling plots. Additionally, the surface sediments in the mobile sand area displayed a peak grain size of 2.250 Φ, accounting for approximately 8.62% of the total soil particles. By contrast, the surface sediments in the clay–sand barrier sampling plots exhibited an average peak grain size of 2.450 Φ, comprising approximately 6.06% of the total soil particles. This result confirms a higher content of fine particle components in the surface sediments of clay–sand barrier sampling plots while the decrease of medium and fine sand contents, compared to the mobile sand area. The disparity in sediment grain size distribution between clay–sand barrier sampling plots and mobile sand area, which is reflected by the variation in grain size composition in the frequency distribution curve, indicates a reduction in the contents of medium and fine sands and an increase in the contents of coarse sand, very fine sand, silt, and clay in the clay–sand barrier sampling plots. Examination of the grain size frequency distribution curves of surface sediments at different positions within the clay–sand barrier sampling plots revealed a pattern of upwind region>middle region>downwind region for the contents of surface sediment grain size in the range of 2.050–4.450 Φ and a pattern of downwind region>middle region>upwind region for the contents of surface sediment grain size in the range of 5.440–11.220 Φ. The disparities in the remaining ranges were not substantial.

The cumulative grain size frequency distribution curves of surface sediments in the study area comprised three segments, corresponding to the creep (with grain size<1.000 Φ), saltation (with grain size of 1.000–3.000 Φ), and suspension (with grain size>3.000 Φ) components. Among these segments, the saltation component exhibited the steepest slope and the highest proportion,
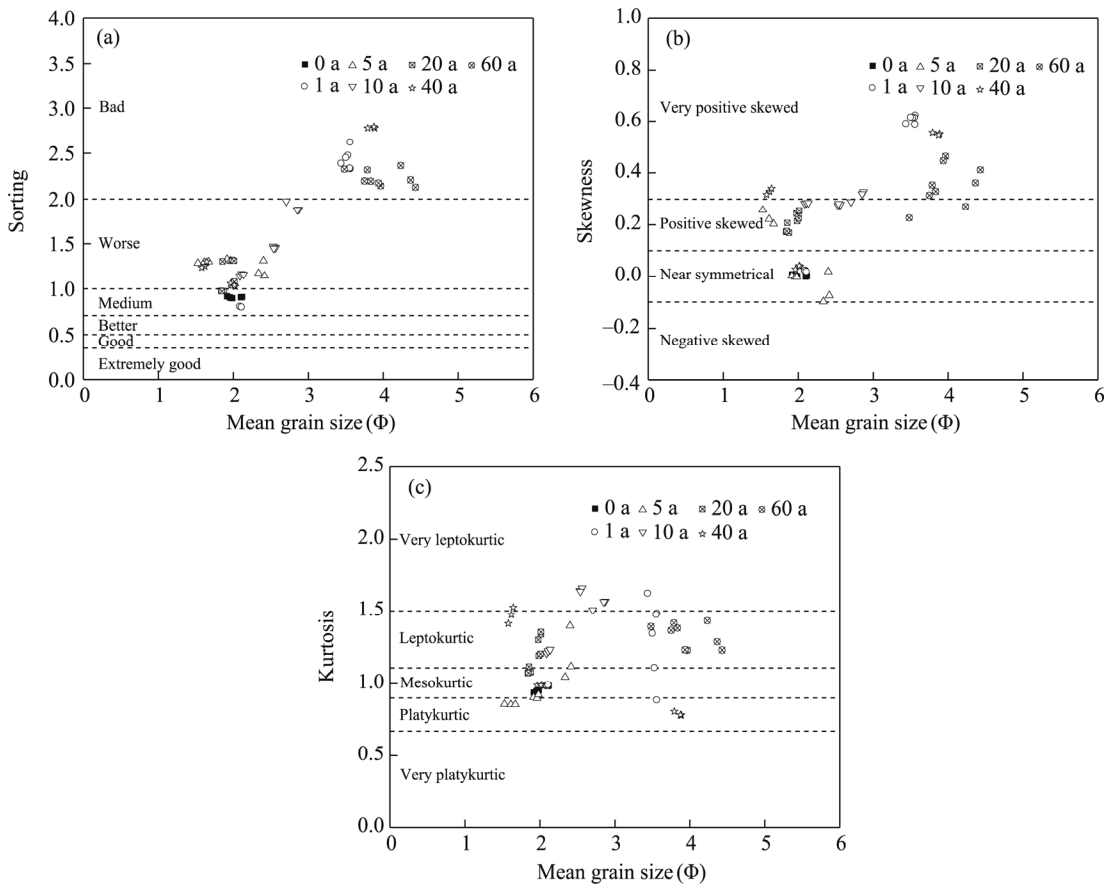
Fig. 4 Relationship between the sorting and mean grain size (a), the skewness and mean grain size (b), and the kurtosis and mean grain size (c) of surface sediments in different sampling plots. The dashed lines in the diagram represents the category lines for each grain size parameter.

exceeding 80.00%, followed by the suspension component. Meanwhile, the creep component had the lowest proportion (Fig. 5). In the study area, the wind force is relatively modest, while the clay–sand barrier is robust, possessing a unique impermeability that results in only fluctuations of airflow over the barriers without the generation of small eddies. Moreover, the peak of the barriers is notably smooth and gentle, facilitating the easy over rolling of sand particles. A marked disparity existed in the grain size composition between clay–sand barrier sampling plots and mobile sand area. The slope of the saltation component in the mobile sand area was more pronounced than that in the clay–sand barrier sampling plots, resulting in an earlier peak in the cumulative grain size frequency distribution curve. The slope values of the cumulative grain size frequency distribution curves among different clay–sand barrier sampling plots were relatively similar, gradually becoming steep in the range of 0.265–4.052 Φ. Notably, the distribution uniformity of grain size composition was comparable among the clay–sand barrier sampling plots with deployment durations of 5, 10, and 20 a but significantly differed from the clay–sand barrier sampling plots with deployment durations of 1, 40, and 60 a. The cumulative grain size frequency distribution curves of surface sediments at different positions initially exhibited a gradual growth pattern, followed by a sudden steep decline at the grain size of approximately 0.066 Φ, rapidly surpassing 80.00% of the cumulative volume percentage. This finding indicates that a large proportion of sediment particles have a grain size greater than 0.066 Φ, resulting in lower contents of coarse and very coarse sand components. The analysis of surface sediments at various positions within the clay–sand barrier sampling plots reveals that the intersection points of the creep component with the saltation component and those of the saltation component with the
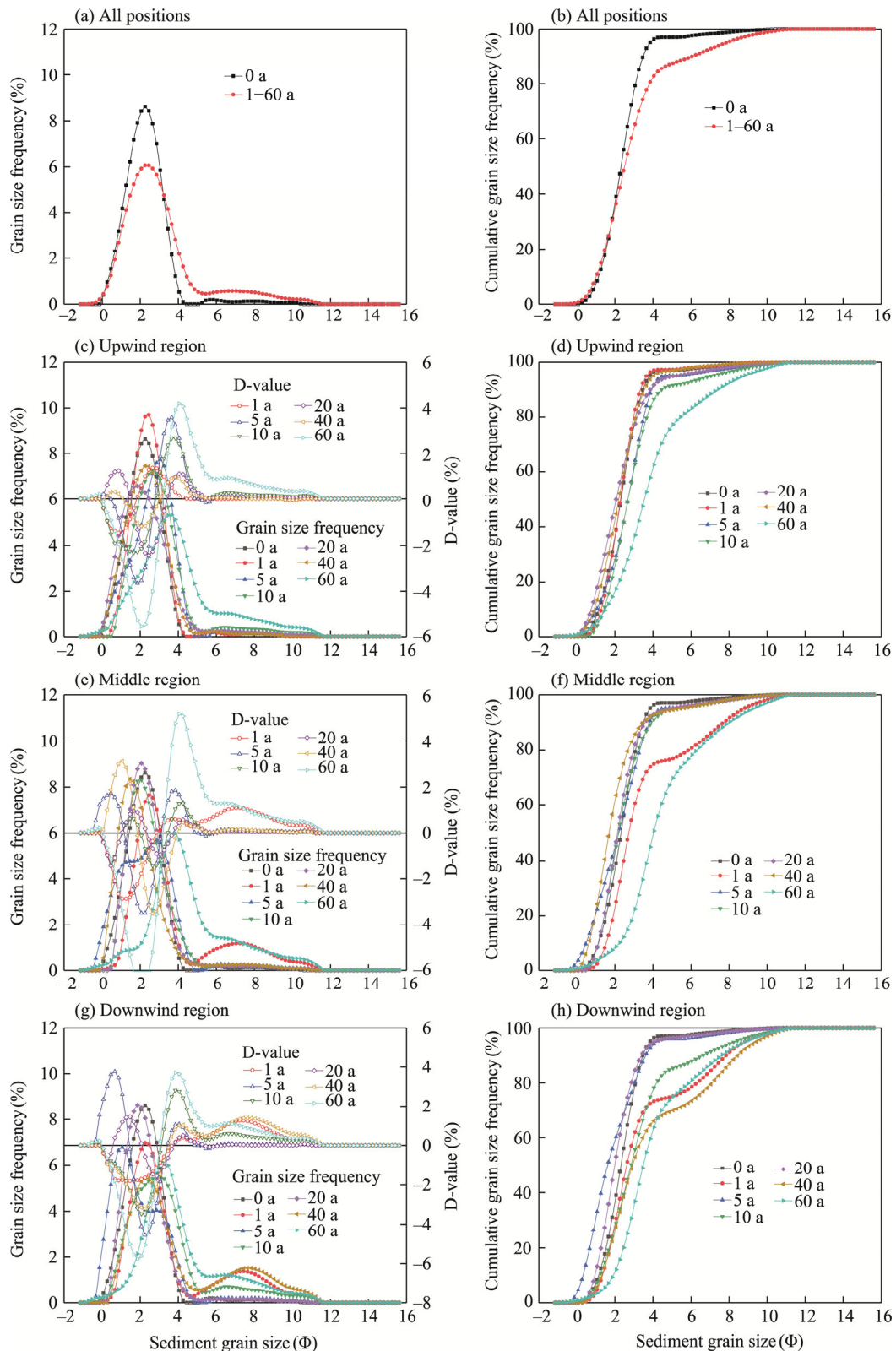
Fig. 5 Grain size frequency distribution curves (a, c, e, and g) and cumulative grain size frequency distribution curves (b, d, f, and h) of surface sediments at all positions and in the upwind (northwest), middle, and downwind (southeast) regions of different sampling plots. D-value means the difference between values in each clay–sand barrier sampling plot and mobile sand area.

suspension component in the cumulative grain size frequency distribution curves occurred at approximately 0.460 and 3.650 Φ, respectively. The slope values of the cumulative grain size frequency distribution curves among different positions followed the order of steepest to gentlest as follows: upwind region>middle region>downwind region. The cumulative grain size frequency distribution curves of surface sediments in the upwind region of the clay–sand barrier sampling plots exhibited the highest slope and reached its peak first, bearing the closest resemblance to the curves in the mobile sand area. The cumulative grain size frequency distribution curves of surface sediments in the downwind region of clay–sand barrier sampling plots possessed a relatively gradual slope and later reached the peak of the curves. This phenomenon also indirectly indicates the mitigating effect of the clay–sand barriers on regional wind speed.

4　Discussion

Soil grain size analysis is a crucial research topic in the study of aeolian sediments (Liao et al., 2021). Conducting research on the grain size distribution of surface soil is valuable for understanding weathering and deposition processes (Ahlbrand, 1979). In the case of Minqin desert area that has implemented sand control measures for over 60 a, the clay–sand barriers alter the sediment grain size distribution inside and outside the barriers by reducing the erosion of wind-blown sand. Furthermore, the clay–sand barriers also affect the contents of easily eroded particles in the surface sediments at different positions within the barriers.

4.1　Effect of clay–sand barriers on the grain size distribution of surface sediments

Minqin desert area is situated between the Tengger Desert and Badain Jaran Desert, characterized by mobile, semi-fixed, and fixed sand dunes (Man et al., 2023). The regional ecological environment is fragile, with sparse vegetation and loose and unstable surface sediments that are prone to aeolian erosion. This region is regarded as one of the main sources of dust storms in China due to its dry climate, unstable atmospheric conditions, limited vegetation, and loose surface sediment materials attributed to water scarcity (Zhao et al., 2011). The clay–sand barrier sampling plots in this study are located in the Minqin desert area on the southeastern edge of the Badain Jaran Desert, where vegetation coverage is low, distances between sampling plots are close, and terrain remains consistent.

Sand barriers help increase soil surface roughness and reduce near-surface wind speed. Unlike conventional sand barriers with certain permeability, such as *Salix psammophila* and straw sand barriers, clay–sand barriers primarily comprise impermeable clay particles, which enhance their obstructive and uplifting effects on airflow (Luo et al., 2023). This condition creates a high threshold wind speed for the transport of sands and gravels. After the deployment of clay–sand barriers, the mechanical composition of surface sediments changes due to alterations in the flow field structure and the deposition of wind-blown sediments (Wang et al., 2022a). This experiment found that the influence of clay–sand barriers on the grain size of surface sediments in the study area was mainly reflected in the increase of fine particle components within the barrier sampling plots (Fig. 5a). Compared to the mobile sand area, the average contents of coarse and medium sands within the barriers after 1 a of the deployment of clay–sand barriers decreased by 3.55% and 11.31%, respectively, while those of clay and silt increased by 2.43% and 5.59%, respectively, indicating the initial manifestation of soil refinement. This finding can be attributed to two main factors: (1) the initial severe aeolian erosion at the top of the newly deployed clay–sand barriers resulted in the shedding of clay particles and a consequent increase in fine particles on the surface; and (2) some clay particles that fell within the surface layer of the sampling plots were retained during the deployment of clay–sand barriers. The study area features a relatively flat topography with low vegetation coverage in the mobile sand area, which is inadequate for obstructing aeolian processes, resulting in a relatively uniform grain size distribution on the surface of the mobile sand area (Fig. 5a). By contrast, the clay–sand barrier structures effectively impede sand flow, capturing the majority of coarse particles on the exterior

of the barriers. This phenomenon leads to a predominance of finer particles in the middle and rear sections within the barriers, which are then widely deposited in the downwind region under the influence of the wind, ultimately resulting in a finer grain size composition on the surface of the clay–sand barrier sampling plots compared to that of the mobile sand area (Fig. 5b). Over time, the mean grain size in the surface sediments within the clay–sand barrier sampling plots becomes finer, revealing a significant increase in the contents of silt and clay and a decrease in the sorting (Fig. 5f). This conclusion is consistent with the findings of Cui et al. (2022), who indicated that fine and medium sands, which are easily eroded, are substantially influenced by aeolian activity. Within the aeolian flow, the erodible particles within the height range of 0–10 cm account for approximately 75.00% of the total particles (Wang et al., 2022b). However, the height of clay–sand barriers is mostly between 25 and 30 cm, and the high barrier height and non-permeable characteristics exacerbate the blockage of surface particles.

Owing to the impediment of sand-laden winds by barriers, a substantial reduction in horizontal wind velocity was observed, indicating the conversion of part of the kinetic energy into an upward force. This conversion diminishes the capacity of the wind to carry heavy, coarse particles, resulting in a preferential interception of such particles outside the barriers and in the upwind region. Meanwhile, light, fine particles are uplifted by the wind, transported, and then ultimately deposited in the downwind region. Multiple notable wind events reinforced this pattern over time (Shahabinejad et al., 2019; Chen et al., 2023). Furthermore, with the continuous recovery of the vegetation within the clay–sand barriers, individual plants can act as barriers against wind-blown sand flow, thereby enhancing the sand-fixing effect (Khalilimoghadam and Bagheri-Bodaghabadi, 2020). Land desertification is a process of soil particle coarsening and nutrient depletion, while the deployment of clay–sand barriers gradually refines the texture of the surface soil, which is contrary to the desertification process and promotes soil restoration (Yao et al., 2016; Luo et al., 2019).

4.2 Effect of clay–sand barriers on the range of eroded particles

The presence of sand barriers alters surface undulation and reduces the intensity of sand and wind activities, thereby impacting the range of sand particle movements (Gao et al., 2004). Bagnold (1941) identified three main forms of sand movement in wind–sand flow: creep, saltation, and suspension. Saltation, which is closely related to suspension and creep movements, is the dominant form of wind–sand flow advancement and serves as a key focal point in the study of granular physics (Zheng and Bo, 2022). In this experiment, the grain size range of surface sediments in the study area was between 1.000 and 3.000 Φ, demonstrating a predominance of fine and medium sand components (Table 3). These components are highly susceptible to aeolian erosion and are sensitive to changes in the flow field. Thus, these components are crucial in determining the relative coarseness of surface sediments within the clay–sand barriers and are particularly influenced by the barriers.

Comparison and analysis of the grain size of surface sediments in the clay–sand barriers sampling plots and mobile sand area in the study area reveals that the proportion of suspension component (>3.000 Φ) in the surface sediments of the clay–sand barrier sampling plots increased by 199.93% compared to the mobile sand area, while the proportion of saltation component generally decreased by 22.15% (Table 3). Additionally, the proportions of suspended and saltation components were high in the downwind region. A general process of particle refinement occurred from the upwind region to the downwind region, reflecting the natural sieving rules of particle selection in the region and confirming the wind protection effect of clay–sand barriers (Chi et al., 2021; Chen et al., 2023).

The sorting of surface sediments in the study area markedly varied, undergoing an overall transition from medium to worse to bad as the deployment duration extended. This transition is primarily due to the gradual deterioration of some barriers in the later stages of the deployment of clay–sand barriers, weakening their wind protection function. This phenomenon results in an uneven distribution of surface sediment particles within the barriers and a wide range of sediment

grain size distribution (Gao et al., 2016). The grain size of surface sediments at different positions of the clay–sand barriers sampling plots was finer than that of the mobile sand area. This phenomenon not only reflects the intercepting effect of clay–sand barriers on wind-blown sand but also indicates the improvement of surface soil structure by the barriers.

Among all the sampling plots in the study area, the grain size composition of surface sediments in the clay–sand barrier sampling plot with deployment duration of 60 a exhibited the most significant difference compared to that in the mobile sand area (Fig. 3). Previous studies have confirmed the close relationship between soil grain size composition and the development and stability of soil crust (Duan et al., 1996). The content of fine particles has a considerable impact on crust formation, while other particle components play a crucial role in crust stability. A higher content of coarse components leads to lower crust stability and higher susceptibility to damage. Conversely, a higher content of fine components enhances soil crust stability (Zhou and Liu, 2022). With the development of the soil crust, considerable improvements in the compaction, bulk density, and other properties of the soil were observed, resulting in changes of transportation and deposition of sands in the region. The protective mechanism of clay–sand barriers has transitioned from the initial "obstruction" approach to a highly comprehensive "obstruction and consolidation" approach (Duan et al., 1996).

4.3   Effectiveness and advantages of clay–sand barriers

The resistance of aeolian erosion offered by clay–sand barriers is a long-term cumulative effect that begins with reductions of wind velocity and sand flow, refinement of soil texture, and progression to the alteration of soil structure, augmentation of soil nutrients, and promotion of vegetation recovery, ultimately culminating in an integrated protective measure that combines engineering with botanical elements (Zhou et al., 2023). Studying changes in surface sediment grain size after the deployment of clay–sand barriers in the study area helps refine the understanding of the wind and sand resistance effects of these barriers.

Different from clay particles, sand particles are coarse and loosely structured, and have minimal water retention and low organic matter contents. Following the deployment of clay–sand barriers, the gradual increase in fine particle components within the surface sediments not only considerably optimizes soil structure but also enhances soil nutrients, creating favorable conditions for the growth of sand-resistant vegetation (Pu, 2010). However, studies have shown that the growth of vegetation within the barriers does not strictly follow a linear relationship with the deployment duration of the barriers (Ding et al., 2018b). In the early stages after the deployment of clay–sand barriers, a noticeable improvement in vegetation, soil moisture, and nutrient conditions can be observed. However, this positive effect gradually weakens over time. Particularly in the later stages, as soil crust coverage substantially increases, this positive effect not only reduces the efficiency of rainfall infiltration but also weakens the replenishment of deep soil by precipitation, making it difficult for plant roots to access water and exerting a certain reverse effect on the growth of plants (Jia et al., 2023).

Moreover, the integrity of sand barriers substantially affects their protective effect (Wang et al., 2023). Clay–sand barriers, which are constructed mainly with clay fragments, have higher density and mass compared to barriers made of straw (Xu et al., 2020). The study by Sun et al. (2012) has shown that after 12 a of deployment, the preservation rate of clay–sand barriers is approximately 65.00%. Although there are different degrees of damage of clay–sand barriers in the study area, such damage is mostly localized and discontinuous. Overall, the protective environment of clay–sand barriers remains relatively stable.

Therefore, the protective function of clay–sand barriers is attributed to a synergy of multiple factors, that is, a virtuous cycle encompassing the reduction of wind speed, soil refinement, and promotion of plant recovery. Future research should comprehensively investigate the wind and sand resistance effects of clay–sand barriers, by considering factors such as sand-resistant plants, soil nutrients, and wind protection efficiency.

Furthermore, clay–sand barriers are particularly suited to regions with abundant clay resources.

In areas where clay particles are scarce, selecting high-quality materials appropriate to the local conditions and conducting a comprehensive assessment of their wind and sand resistance efficiency, sustainability, economic cost, and potential secondary pollution remains imperative before large-scale application (Zhang et al., 2018). Specific to Minqin desert area, clay–sand barriers possess special advantages, representing a mature artificial sand control measure. In the future, promptly maintaining any damaged areas of clay–sand barriers is essential to ensuring the sustained efficacy of their protective benefits.

5 Conclusions

From the perspective of surface sediment grain size, this study investigated the aeolian erosion resistance of clay–sand barriers with different deployment durations in Minqin desert area to promote the optimization of artificial sand control projects in arid desert areas. The deployment of clay–sand barriers substantially enhanced the fine particle contents of surface sediments. With the passage of time, the contents of fine particles in the surface sediments of clay–sand barrier sampling plots, which comprise very fine sand, silt, and clay, displayed a fluctuating upward trend, while the contents of coarser particles such as fine and medium sands showed a fluctuating downward trend. These changes became increasingly and highly pronounced after 10 a of deployment. The interception of sand flow by clay–sand barriers and the selective influence of the dominant wind in the region collectively altered the spatial distribution of surface sediment particles. The clay–sand barriers have a greater impact on coarser particles due to their obstructive effect, while the selective influence of the dominant wind plays a more significant role in affecting finer particles. Clay–sand barriers demonstrate their anti-erosion efficacy by reducing wind speed, obstructing sand flow, and promoting the refinement of soil particles on the surface. Future efforts to repair the clay–sand barrier protection systems should focus on the restoration of damaged barriers in the upwind region to maintain and extend the protective effects of clay–sand barriers, ensuring the enduring benefits of windbreak and sand fixation.

Conflict of interest

ZHAO Wenzhi is an editorial board member of Journal of Arid Land and was not involved in the editorial review or the decision to publish this article. All authors declare that there are no competing interests.

Author contributions

Conceptualization: ZHAO Wenzhi; Data curation and software: SONG Dacheng; Methodology: SONG Dacheng, WANG Lide, MA Quanlin; Investigation and formal analysis: SONG Dacheng, WEI Lemin, WU Hao; Writing - original draft preparation: SONG Dacheng; Writing - review and editing: SONG Dacheng, ZHAO Wenzhi; Funding acquisition: ZHAO Wenzhi, LI Guangyu, WANG Lide, MA Quanlin; Resources: YANG Jingyi; Supervision: ZHAO Wenzhi. All authors approved the manuscript.

References

Ahlbrandt T S. 1979. Textural parameters of aeolian deposits. In: Mckee E D. A Study of Global Sand Sea. U.S. Geological Survey Professional Paper 1052, 21–51.

Bagnold R A. 1941. The Physics of Blown Sand and Desert Dunes. London: Methuen.

Bruno L, Coste N, Fransos D, et al. 2018. Shield for sand: an innovative barrier for windblown sand mitigation. Recent Patents on Engineering, 12(3): 237–246.

Cao B, Sun B P, Gao Y, et al. 2007. Effect of high-banded *Salix psammophila* sand-barriers on reduction of wind speed. Science of Soil and Water Conservation, 5(2): 40–45. (in Chinese)

Chang Z F, Zhong S N, Han F G, et al. 2000. Research of the suitable row spacing on clay barriers and straw barriers. Journal of Desert Research, 20(4): 455–457. (in Chinese)

Chen J P, Yu Z Y, Yang F, et al. 2023. Particle size characteristics of sandstorm and surface sand at Tazhong area of Taklimakan Desert, China. Journal of Desert Research, 43(2): 150–158. (in Chinese)

Chi Z, Xu X Y, Liu K L, et al. 2021. Study on soil particle size characteristics and spatial pattern of sand deposition in two types of sand barriers. Journal of Soil and Water Conservation, 35(2): 113–121. (in Chinese)

Cui G P, Xiao C L, Lei J Q, et al. 2023. China's governance: Strategy choice and future vision for combating desertification. Bulletin of Chinese Academy of Sciences, 38(7): 943–955. (in Chinese)

Cui J, Dang X H, Wang J, et al. 2022. Characteristics of soil particle size and organic matter after five years of laying different specifications of degradable sand barriers. Research of Soil and Water Conservation, 29(2): 92–98. (in Chinese)

Ding A Q, Xie H C, Xu X Y, et al. 2018a. Influence of three different mechanical sand barriers to sand dune vegetation, soil particle size and moisture content in late stage. Soil and Water Conservation in China, 5: 59–63, 69. (in Chinese)

Ding Y L, Gao Y, Wang J, et al. 2018b. Effects of biodegradable poly lactic acid sand barriers on surface sediment grain-size characteristics at sand dunes. Journal of Desert Research, 38(2): 262–269. (in Chinese)

Dong Z B, Li Z S. 1998. Wind erodibility of aeolian sand as influenced by grainsize parameters. Journal of Soil Erosion and Soil and Water Conservation, 4(4): 1–5, 12. (in Chinese)

Dong Z W, Mao D L, Ye M, et al. 2022. Fractal features of soil grain-size distribution in a typical *Tamarix* cones in the Taklimakan Desert, China. Scientific Reports, 12: 16461, doi: 10.1038/s41598-022-20755-x.

Duan Z H, Liu X M, Qu J J, et al. 1996. Study on formation mechanism of soil crust in the Shapotou area. Arid Zone Research, 13(2): 31–36. (in Chinese)

Folk R L, Ward W C. 1957. Brazos River bar: a study in the significance of grain size parameters. Journal of Sedimentary Research, 27(1): 3–26.

Gao G L, Ding G D, Zhao Y Y, et al. 2016. Characterization of soil particle size distribution with a fractal model in the desertified regions of Northern China. Acta Geophysica, 64(1): 1–14.

Gao Y, Qiu G Y, Ding G D, et al. 2004. Effect of *Salix psammophila* checkerboard on reducing wind and stabilizing sand. Journal of Desert Research, 24(3): 365–370. (in Chinese)

Jia H F, Jia R L, Wu X L, et al. 2023. Effects of biocrust on soil swelling in arid desert. Journal of Desert Research, 43(2): 28–36. (in Chinese)

Khalilimoghadam B, Bagheri-Bodaghabadi M. 2020. Factors influencing the relative recovery rate of dunes fixed under different sand-fixing measures in southwest Iran. Catena, 194: 104706, doi: 10.1016/j.catena.2020.104706.

Labiadh M T, Rajot J L, Sekrafi S, et al. 2023. Impact of land cover on wind erosion in arid regions: a case study in southern Tunisia. Land, 12(9): 1648, doi: 10.3390/land12091648.

Li X R, Ma F Y, Xiao H L, et al. 2004. Long-term effects of revegetation on soil water content of sand dunes in arid region of Northern China. Journal of Arid Environments, 57(1): 1–16.

Liao K H, Lai X M, Jiang S Y, et al. 2021. Estimating the wetting branch of the soil water retention curve from grain-size fractions. European Journal of Soil Science, 72(1): 215–220.

Luo X Y, Li J R, Tang G D, et al. 2023. Interference effect of configuration parameters of vertical sand-obstacles on near-surface sand transport. Frontiers in Environmental Science, 11: 1215890, doi: 10.3389/FENVS.2023.1215890.

Luo Y X, Liu R T, Zhang J, et al. 2019. Soil particle composition, fractal dimension and their effects on soil properties following sand-binding revegetation within straw checkerboard in Tengger Desert, China. Chinese Journal of Applied Ecology, 30(2): 525–535. (in Chinese)

Ma R, Liu H J, Ma Y J, et al. 2013. Influences of sand fountain on sand-fixation of mechanical sand barriers. Journal of Soil and Water Conservation, 27(5): 105–108, 114. (in Chinese)

Man D Q, Tang J N, Yang X M, et al. 2023. The change characteristics of 10 typical desert plant populations in Minqin desert area in 1960 to 2021. Journal of Desert Research, 43(6): 20–28. (in Chinese)

Meng J, Sun H, Teng C, et al. 2023. Improvement and application on the estimation model of windbreak and sand fixation function based on remote sensing soil moisture factors. Chinese Journal of Applied Ecology, 34(10): 2788–2796. (in Chinese)

Pan X, Wang Z Y, Gao Y. 2020. Effects of Compound sand barrier for habitat restoration on sediment grain-size distribution in Ulan Buh Desert. Scientific reports, 10(1): 2566, doi: 10.1038/s41598-020-59538-7.

Piao Q H. 2010. Effect of different sand barriers on wind-break and sand fixation. PhD Dissertation. Beijing: Beijing Forestry University. (in Chinese)

Qiao Y S, Guo Z T, Hao Q Z, et al. 2006. The particle characteristics of the Miocene-Pleistocene loess-paleosol sequence and their implications for the genesis. Scientia Sinica (Terrae), 36(7): 646–653. (in Chinese)

Shahabinejad N, Mahmoodabadi M, Jalalian A, et al. 2019. The fractionation of soil aggregates associated with primary particles influencing wind erosion rates in arid to semiarid environments. Geoderma, 356: 113936, doi: 10.1016/j.geoderma.2019.113936.

Song J, Chun X, Bai X M, et al. 2016. Review of grain size analysis in China desert. Journal of Desert Research, 36(3): 597–603. (in Chinese)

Sun T, Liu H J, Zhu G Q, et al. 2012. Timeliness of reducing wind and stabilizing sand functions of three mechanical sand barriers in arid region. Journal of Soil and Water Conservation, 26(4): 12–16, 22. (in Chinese)

Wang F, Liu S X, Jiang Y J, et al. 2023. Research on the effect of sand barriers on highways in desert areas on sand control. Sustainability, 15(18): 13906, doi: 10.3390/su151813906.

Wang H Y, Tong W, Liu J B, et al. 2022a. Soil wind erosion resistance analysis for soft rock and sand compound soil: A case study for the Mu Us Sandy Land, China. Open Geosciences, 14(1): 824–832.

Wang Q Q, Tang J N, Yang Z H, et al. 2017. Sand fixing effects of embedded plastic banding sand-barrier and its potential application. Soil and Water Conservation in China, (4): 35–38, 69. (in Chinese)

Wang T, Qu J J, Niu Q H. 2020. Comparative study of the shelter efficacy of straw checkerboard barriers and rocky checkerboard barriers in a wind tunnel. Aeolian Research, 43: 100575, doi: 10.1016/j.aeolia.2020.100575.

Wang Y S, Wang D D, Yu X X, et al. 2022b. Emissions of biological soil crust particulate matter and its proportion in total wind erosion. Land Degradation & Development, 33(16): 3118–3132.

Xu Z W, Mason J A, Xu C, et al. 2020. Critical transitions in Chinese dunes during the past 12,000 years. Science Advances, 6(9): 8020, doi: 10.1126/sciadv.aay8020.

Yao J Z, Liu T X, Tong X, et al. 2016. Soil particle fractal dimension in the dune meadow ecotone of the Horqin Sandy Land. Journal of Desert Research, 36(2): 433–440. (in Chinese)

Zhang C L, Shen Y P, Li Q, et al. 2018. Sediment grain-size characteristics and relevant correlations to the aeolian environment in China's eastern desert region. Science of the Total Environment, 627: 586–599.

Zhang Z S, Dong Z B. 2012. The effect of wind erosion on the surface particle size. Journal of Arid Land Resources and Environment, 26(12): 86–89. (in Chinese)

Zhao M, Zhan K J, Yang Z H, et al. 2011. Characteristics of the lower layer of sandstorms in the Minqin desert-oasis zone. Science China Earth Sciences, 54(5): 703–710.

Zhao P, Xu X Y, Zhang Y N, et al. 2023. Age structure and its dynamics of artificial *Haloxylon ammodendron* population in Minqin oasis-desert ecotone. Acta Ecologica Sinica, 43(14): 6069–6079. (in Chinese)

Zheng X J, Bo T L. 2022. Representation model of wind velocity fluctuations and saltation transport in aeolian sand flow. Journal of Wind Engineering and Industrial Aerodynamics, 220: 104846, doi: 10.1016/J.JWEIA.2021.104846.

Zhou H, Liu Y X. 2022. Effects of soil crusts on physicochemical properties of shallow soil in alpine sandy area. Journal of Arid Land Resources and Environment, 36(8): 154–160. (in Chinese)

Zhou Y G, Li H Y, Wu Z F, et al. 2023. Sand fixation mechanism and effect evaluation of sand barriers in Mu Us sandy land, China. Chinese Science Bulletin, 68(11): 1312–1329. (in Chinese)